Macroscopic and microscopic dynamics of a pedestrian cross-flow: Part I, experimental analysis

Francesco Zanlungo [a,b,*], Claudio Feliciani [c], Zeynep Yücel [b], Katsuhiro Nishinari [c,d], Takayuki Kanda [e]

[a] *International Professional University of Technology in Osaka, 3-3-1 Umeda, Kita-ku, 530-0001, Osaka, Japan*
[b] *Graduate School of Natural Science and Technology, Okayama University, 3-1-1 Tsushima-naka Kita-ku, 700-8530, Okayama, Japan*
[c] *Research Center for Advanced Science and Technology, The University of Tokyo, 4-6-1 Komaba, Meguro-ku, 153-8904, Tokyo, Japan*
[d] *Department of Aeronautics and Astronautics, Graduate School of Engineering, The University of Tokyo, 7-3-1 Hongo, Bunkyo-ku, 153-8656, Tokyo, Japan*
[e] *Graduate School of Informatics, Kyoto University, Yoshidahonmachi, Sakyo-ku, 606-8317, Kyoto, Japan*

ARTICLE INFO

ABSTRACT

In this work we investigate the behaviour of a human crowd in a cross-flow by analysing the results of a set of controlled experiments in which subjects were divided into two groups, organised in such a way to explore different density settings, and asked to walk through the crossing area. We study the results of the experiment by defining and investigating a few macroscopic and microscopic observables. Along with analysing traditional indicators such as density and velocity, whose dynamics was, to the extent of our knowledge, poorly understood for this setting, we pay particular attention to walking and body orientation, studying how these microscopic observables are influenced by density. Furthermore, we report a preliminary but quantitative analysis on the emergence of self-organising patterns (stripes) in the crossing area, a phenomenon that had been previously qualitatively reported for human crowds, and reproduced in models, but whose quantitative analysis with respect to density conditions is, again according to our knowledge, a novel contribution.

1. Introduction

Pedestrian facilities can be found in any part of the world where people transit, move or gather. Train stations, stadia or airports are just a few examples of such structures, but shopping malls or other commercial facilities also attract a large number of customers, thus requiring a design that can guarantee safety and comfort of their occupants. Religious events or concerts also require meticulous planning, especially when a large crowd is expected over a short period of time in temporary facilities built to accommodate participants.

The design of pedestrian facilities has been traditionally based on the experience gained from on-site personnel managing them. Nonetheless, data gained on pedestrian and crowd motion over the last 50 years helped defining standards and regulations, which have contributed in greatly increasing the safety of buildings especially in case of evacuations. In addition, simulation software is also playing an increasingly dominant role in the design of pedestrian facilities (Lovreglio et al., 2020). The increasing role of models can be also confirmed by the creation of standards for the validation of those designed for the simulation of emergency evacuations (International Organization for Standardization, 2020). In addition, simulation software is also used to study pedestrian flow lines in normal situations with the aim to improve pedestrian traffic and thus ensure a better experience for its users.

However, as already briefly stated above, the advances in the study of pedestrian dynamics over the last decades are also related to the increasing availability of empirical data that has helped in the definition of new theories, standards and constituted the base upon which validation of numerical models is performed. The most representative example is the study of the fundamental diagram of pedestrian traffic. Based on this framework, developed from knowledge gained on vehicular traffic but backed by quantitative measurements on pedestrian motion, Fruin defined the LOS (Level Of Service), which is still one of the most used criteria to classify quality of pedestrian areas (Fruin, 1971). Although the universality of the fundamental diagram is often debated, its validity is not under discussion and has allowed to identify differences in pedestrian motion related to diverse factors such as age, gender and culture (Chattaraj et al., 2009; Fujita et al., 2019; Ye et al., 2021; Subaih et al., 2020; Cao et al., 2016).

Initially, empirical data on collective motion were mostly collected in public facilities, which can be seen as the most logical choice since they represent the "natural habitat", i.e. the ecological context where pedestrians move (Weidmann, 1993). However, to study the very fundamental mechanisms of collective motion and remove the influence of external variables difficult to control in public facilities, controlled experiments also started to be considered and an increasing number has been performed over the last few decades (Haghani and Sarvi, 2018). In general, it can be said that the scope of supervised experiments is to manipulate each variable affecting collective motion in public spaces independently, thus allowing to better understand its influence before considering the combination of multiple factors. For instance, route choice (Crociani et al., 2016), exit selection (Bode et al., 2015), disabilities and/or walking impairment (Geoerg et al., 2019), collaborative vs competitive behaviours (Von Krüchten and Schadschneider, 2017), level of competitiveness (Feliciani et al., 2020b), social norms (Zanlungo et al., 2012), social bonds and relationships (Ye et al., 2021; Zanlungo et al., 2014, 2015; Zanlungo and Kanda, 2015; Zanlungo et al., 2017, 2019, 2020) or available information (Feliciani et al., 2020a) are examples of variables which are better studied in supervised experiments or by carefully selecting a specific area of a public space where influence of other factors is minimal.

When it comes to physical aspects of collective motion, one of the most simple and common supervised experiments is represented by the single-file walking in a loop. Despite the very simple geometry, effectively making motion strictly uni-dimensional, several important properties of pedestrian dynamics can be obtained, from the previously mentioned fundamental diagram to more subtle aspects related to stepping and locomotion (Chattaraj et al., 2009; Jelić et al., 2012; Wang et al., 2018; Subaih et al., 2020; Cao et al., 2016). In addition, evacuation (or more generally egress) also represents a commonly studied scenario (Seyfried et al., 2009; Adrian et al., 2020; Feliciani et al., 2020b). Uni-directional experiments were also performed with different corridor widths thus allowing the consideration of more complex interaction among pedestrian (Zhang et al., 2012). Although bottleneck/egress and the corridor-shaped uni-directional flow take complexity one step further from the single-file geometry, they all represent quite simple conditions in terms of collision avoidance since headway is the most important parameter upon which speed is adapted, with limited changes in longitudinal direction and shoulder orientation.[1]

Furthermore, a number of studies were performed on bi-directional flows, where people from two directions meet in a delimited path, such as in a corridor or a crosswalk (Zhang et al., 2012; Feliciani and Nishinari, 2016; Murakami et al., 2021). The increasing complexity given by the existence of frontal collision avoidance leads to the creation of self-organised structures, lanes in the case of a bi-directional flow, which are the results of an optimisation strategy occurring on a collective level with the aim of limiting potential collisions. Even this comparatively simple scenario is still not fully understood and simulations often fail in reproducing experimental results, typically either leading to an overly straightforward formation of lanes or running into a deadlock at relatively low densities. This shows that even a simple case like the bi-directional flow is worth being studied and, as stated above, knowledge gained from the understanding of its underlying principles can have consequences on the practical aspects and applications.

With this said, it is also worth adding that the full complexity of the bi-directional case is only at play during the time in which lanes are forming. Once the crowd divides into well distinguished lanes, the motion is basically uni-directional, with each lane being potentially considered as (almost) independent from the others (Feliciani et al., 2018). For this reason, the knowledge obtained by studying the bi-directional scenario may not be generalised in a straightforward

way. For example, models focusing on "following strategies" could describe very well self-organisation in bi-directional flows while failing to reproduce proper collision avoidance in general settings.

In the discussion provided above controlled experiment (or, more in general, simple geometries) were presented as a solution to obtain data to be used in research and to validate numerical models. It is nonetheless worth pointing out their limitations. For instance, people are known (or at least they are believed) to behave quite differently in controlled experiments compared to the ecological context. Thus, depending on the purpose of the study, collecting data in public facilities would be preferable. But, on the other side, controlled experiments allow to remove potential influences related to the surrounding environment which are difficult to quantify in real-life observations. As such, a well designed controlled experiment may identify fundamental aspects of crowd motion, which could help explaining the dynamics observed in an ecological context, where additional factors need to be accounted in addition to the fundamental dynamics.

From what discussed above we may assume that the cross-flow, a condition where two groups of people coming from different directions cross in a delimited space, represents a good test-bed to study collision avoidance in controlled conditions. Although, as we discuss below, self-organising patterns are present also in a crossing scenario, the geometry of the problem does not allow for a complete spatial separation of different flows, and pedestrians (and participants) need to continuously perform (relatively) complex avoidance behaviour to navigate the crossing area. In addition, it is worth mentioning that intersections are a common element of pedestrian infrastructures and accidents occurred in the past (such as the 1993 Lan Kwai Fong Accident in Hong Kong Lee and Hughes, 2005; Feliciani et al., 2022b), thus highlighting the importance of this geometry for the sake of safety.

For these reasons, in this work, we study the behaviour of pedestrians in a cross-flow. The geometry consists of a crossing area where two orthogonal corridors, each characterised by a uni-directional flow, meet, and interactions among pedestrians are observed and studied. Again, we should point out that these are extremely idealised and simplified conditions. In the real world crossing flows are not necessarily orthogonal and even when such a condition occurs, people may have different destinations and thus some of them may turn left or right, limiting the proportions of those aiming to the opposite side of the crossing area. Nevertheless, given what discussed above, we believe the cross-flow scenario is a good trade-off between a too simple geometrical setup and a completely realistic behaviour in terms of collision avoidance. In that regard, the complex interactions among participants, requiring both anticipatory and collision avoidance abilities, could reproduce well what is observed in a real world context (possibly excluding the fact that in public spaces people often move in groups, while experiments only considered individual behaviour).

Despite the remarkable properties listed above, only few studies considered the cross-flow geometry in the frame of controlled experiments (although it is however often considered in numerical models). The few studies that did consider it mostly focused on macroscopic quantities, often with the aim to compare it with other geometries, without discussing microscopic properties which we consider to be worth studying in light of the non-trivial collision avoidance mechanisms involved (Wong et al., 2010; Cao et al., 2017, 2018).

As stated above, qualitative observations and preliminary studies suggest that self-organising patterns emerge in the cross-flow, ultimately reducing the interactions between streams and optimising the overall flow. More precisely, the occurrence of "diagonal stripes" has been reported, but little quantitative evidence has been given to support their emergence (Naka, 1977; Ando et al., 1988; Helbing et al., 2005). On the other side, diagonal stripes are used in "centrally organised" marching parades (Rokko High School, 2017), where well-trained people enter the crossing area in a predetermined formation thus preventing any collision and leading to an aesthetically appealing motion. Theoretical justification for the emergence of such a pattern

---

[1] With the possible exception of extreme high-density conditions where shoulder orientation is constrained by available space.

can be found in Cividini et al. (2013a), Cividini and Appert-Rolland (2013) (using a discrete lattice model), Cividini et al. (2013b) (using a mean field approach), Hittmeir et al. (2016) (using a partial differential equation model) and Totzeck (2019) (using an anisotropic agent model). In addition, such pattern has also been recently reported in an experimental work (Mullick et al., 2022) whose analysis focused on the relationship between crossing angles and stripe orientation. On the other hand, as detailed later on, in this work we focus on density conditions and crossing angle is kept constant at $\pi/2$. Finally, it is worth mentioning that although stripes have been typically presented as regular well-defined structures (especially in simulation models), they are expected to appear highly irregular in real crowds (in particular when density is very low or very high). To study such kind of irregular formations, a definition describing "stripe" shape is needed and this is best done employing clustering algorithms, something that we indeed intend to perform in a future work. Nevertheless, the fundamental nature of the problem is geometrically simple and an initial analysis can be carried out based only on relative angles between first neighbours (as defined in Appendix A and formalised in Eqs. (A.22) and (A.24)). As we will show, these observables provide some initial evidence on stripe formation and suggest conditions for their emergence.

In this work, we aim to study details of the microscopic and macroscopic dynamics of the cross-flow. More specifically, we are going to consider six different experimental conditions of two flows crossing orthogonally through a central square. For each condition, pedestrian density in both flows was changed (while maintaining density *equal between the flows*) and a number of repetitions were performed to ensure sufficient statistical validity. Results are based on the analysis of nine different macroscopic and microscopic observables (rigorously defined below). Some of them are quite common in the study of crowd dynamics (e.g. temporal change in density, speed distribution), but others have been studied to a lesser extent, such as the probability distribution of distances between first neighbours (either in the same or in the crossing flow) or the distribution of the velocity direction. Some additional features have been, to our knowledge, studied to a very limited extent, such as the distribution of relative position angles between first neighbours (either in the same and in the crossing flow). Finally, believing it may play an important role at high densities, we also obtained data regarding body orientation, which could help in deepening the understanding on its role in collision avoidance. Consequently, body orientation and its deviation with respect to the velocity direction are also studied, adding to the list of rarely studied properties of pedestrian motion.

2. Experiments

2.1. Experimental setup

At the scope of collecting empirical data on the behaviour of crowds in a cross-flow scenario, an experimental campaign was organised recruiting students as participants. Two waiting/starting lanes having an equal width $w = 3.0$ m were prepared, each creating a similar uni-directional flow. These two flows were directed in such a way to have them crossing perpendicularly in a specific area where the trajectories of participants were collected. Experiments were conducted outdoors on the Tokyo university campus on December 7th, 2019. To protect participants from the rain roof-covered parts of the building were used and, due to space limitations, a starting lane had to be bent. The experimental setup is schematically presented in Fig. 1(a) and in addition a top-view image of the experimental setup is also provided in Fig. 1(b) .

To allow an accurate setup of crowd density in each starting area and yet get a uniform distribution of participants, starting lines were drawn on the ground and participants were asked to freely take position between the external perimeter of the crossing area (whose borders delimited by magenta lines are clearly visible in the image of Fig. 1(b))

and the line determining the end of the waiting area (i.e. the grey thick line shown in Fig. 1(a) whose distance from the crossing area is indicated as l). Staff members checked that subjects disposed themselves in a uniform way. The control of density in the crossing area was consequently achieved by setting different lengths l in the starting areas (i.e. moving the location of the grey line in Fig. 1(a)). Namely, six different lengths have been considered: $l = 36.0$ m, $l = 18.0$ m, $l = 9.0$ m, $l = 6.0$ m, $l = 4.5$ m and $l = 3.6$ m.

This configuration was planned expecting a total number of 54 participants, which would lead to starting area densities $\rho_I = 0.25$, $\rho_I = 0.5$, $\rho_I = 1$, $\rho_I = 1.5$, $\rho_I = 2$ and $\rho_I = 2.5$ ped/m^2 (following the same order given for the lengths l above). However, a slightly higher number of participants showed up on the day of the experiments: 56, 2 more than originally expected[2]. As a consequence, real densities were slightly higher (3.7% higher to be precise). Nonetheless, to keep presentation of the results simple, we kept the original densities to label each experiment, also considering that those are simply initial conditions and densities really observed in the crossing area are measured in detail from the collected data.

For each initial density condition, 6 repetitions were performed, although this number was increased to 8 for the configuration having the lowest density ($\rho_I = 0.25$ ped/m^2), see also Table 1 for details. To limit the capability of participants to develop efficient strategies through a learning process, configurations were not performed in increasing/decreasing order but following a shuffled schedule (again details are provided in Table 1). Considering that participants simply walked straight in the starting areas, marking was only performed delimiting each region with coloured signs on the ground. However, due to the strong interactions observed in the crossing area and its importance in the frame of data collection and analysis, this area has been delimited using chain partitions (see Fig. 1(b)).

2.2. Experimental procedure

An overall number of 56 participants voluntarily applied for the experiments. Only males were recruited since other planned experiments had male-only conditions[3] (and partially to avoid possible issues arising from body contact at high densities.[4]) Instructions to the participants were simple and yet clear. They were asked to line up in front of the entrance of the (magenta) crossing area uniformly occupying the whole space available in the starting area (again, this being defined as the area between the central crossing and the end line shown in grey in Fig. 1(a)). When participants finished taking position in the starting area, a "start" signal was given so that they start walking towards the central crossing. Both groups had to walk straight, pass through the crossing area and keep walking for a short distance after leaving it (to avoid congestion due to stopping participants). Staff on-site helped to ensure a uniform distribution and to avoid participants taking repeatedly similar positions (front/back positions are typically

---

[2] Based on previous experiences with participants not showing up the day of the experiments without informing the organisers in time, a higher than needed number of participants was recruited, i.e. 56 people. Since they all showed up and the total number was even, we decided to get them all involved to increase the sample size without affecting results.

[3] A male-only condition was chosen instead of a female-only one since other experiments in the same session (Murakami et al., 2021) were partially aimed to compare results with a previous work (Feliciani and Nishinari, 2016). Also, the proportion of males is quite high in the department with which organisers are affiliated, making recruitment of males easier.

[4] The dynamics of a mixed-gender crowd could be significantly different, due to greater variation in body size, preferred speed, and possibly even collision avoidance norms; nevertheless we believe that even the results arising from a same-gender crowd are novel and of interest to the crowd dynamics research community.
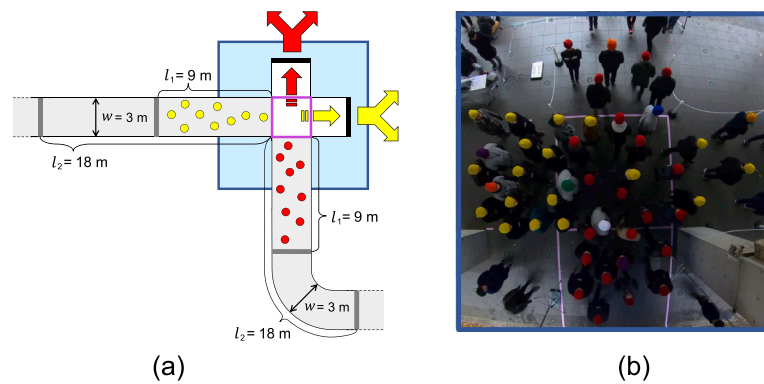
Fig. 1. (a): schematic representation of the experimental area. For the sake of simplicity, only a small number of pedestrians is represented. The crossing area is the square bordered in magenta on the image taken from the camera as shown in (b). The end of the waiting area is shown using a grey line and its length is indicated as l. In this example two settings are shown: $l_1 = 9$ m and $l_2 = 18$ m. In the representation shown in (a) participants occupy the starting area having a length $l = 9$ m. Note that for each experimental run, the lengths of the waiting area in the two lanes were the same. (b): frame relative to a specific experiment with $\rho_I = 2$ ped/m² (i.e., length of the starting area was 4.5 m). The image corresponds approximately to the blue area given in the schematic representation in (a). The participants wearing caps different from red or yellow had been equipped with tablets to measure their body orientation. (For interpretation of the references to colour in this figure legend, the reader is referred to the web version of this article.)

Table 1
Summary of relevant information on experimental procedure and collected data. Nominal density refers to the descriptive value used in this work, real to the effective density. Units for density and distance are omitted for the sake brevity, they are ped/m² and m, respectively. Number of valid orientation samples refer to trajectories associated with body orientation satisfying all requirements to couple them and ensure quality standards. Note that orientation samples refer to the sum over all the repetitions corresponding to a given density condition. Ideally the total number of samples should be equal to the number of participants equipped with tablets and whose recognition was possible (i.e., 9 participants) multiplied by the number of repetitions, although such number of samples is usually lower due to the issues explained in the text.

Starting density		End line distance	Number of repetitions	Execution order	Valid body orientation samples
Nominal	Real				
0.25	0.26	36	8	10, 11, 12, 13, 20, 31, 32, 38	60
0.5	0.52	18	6	4, 5, 6, 21, 30, 33	52
1	1.04	9.0	6	1, 2, 3, 22, 29, 34	53
1.5	1.56	6.0	6	14, 15, 16, 23, 28, 35	53
2	2.07	4.5	6	7, 8, 9, 24, 27, 36	52
2.5	2.59	3.6	6	17, 18, 19, 25, 26, 37	54

preferred). In addition, staff at the exit encouraged participants to keep walking past the crossing area.

Experimental procedures were approved by the Ethical Commission of the university of Tokyo and conform with the Declaration of Helsinki. Participants received clear information on the nature of the research, methods employed and disclosed data. After a briefing, they gave written permission for participation and data acquisition and received a remuneration in accordance to the university's policies.

2.3. Data acquisition and processing

A camera was placed approximately 6 m right above the centre of the crossing area to record the dynamics observed during the experiments. Resolution was set at 3000 × 4000 pixel and frame rate at 30 fps. Trajectories were extracted from the recorded videos using the PeTrack software (Boltes et al., 2010; Boltes and Seyfried, 2013) employing hats with different colours worn by participants as markers. It is important to remark that the software employed allows to take into account both camera distortion (due to the wide-lens used) and perspective. This means that obtained trajectories are representative of planar motion and relative to the projection of people's head to the ground.

Since body orientation is an important part of the analysis presented hereafter, the following approach was taken to gain precise information on this quantity. 10 participants were given a tablet (Nexus 7, 2013) which was fixed to their body using a bib (see also Nagao et al., 2018 for more details). However, one of the participants equipped with tablets mistakenly used a red cap intended to be used by participants without tablet (instead of the white colour assigned to him), thus making individual recognition impossible (details will follow later). Consequently, only data relative to 9 participants have been available to study body orientation in relation to moving direction.

The tablet recorded the movements in the upper body part and more specifically the pedestrian chest orientation, which, except in cases of strong torsion, is expected to provide a reliable estimate of shoulder orientation (often regarded as the proxy for body orientation Willems et al., 2020). Tablet (body) orientation was obtained by making use of the inbuilt gyroscope sensor. Previous research (Feliciani and Nishinari, 2022) showed that errors in terms of precision and accuracy of the gyroscope sensor are below 1%. This allows obtaining an angle given the initial orientation and integrating the measured angular velocity over time. Due to the small error, dead-reckoning is thus not an issue for short time measurements such as in the case of this experiment.

From the details presented above, it should be clear that to properly record body orientation it is necessary to know its initial value. For this reason, participants wearing a tablet were asked to orientate towards the crossing area (i.e., in such a way that the normal to their chest was aligned with the corridor's axis) before the start of the experiments so that angles could be computed accurately. However, as it could be possible that some participants did not follow the instructions properly, to verify the reliability of body orientation information, we overlapped the video recording of the experiments with "animations" that used ellipse shaped "virtual pedestrians" whose positions and orientations were given according to our tracking process, and proceeded to eliminate the few instances in which body orientation appeared to be unreliable (see also Table 1 for details). In addition, in some instances the gyroscope sensor failed to collect data for almost one second. Since angle orientation is obtained by integration, in such cases, this information is lost, requiring to neglect the record. Due to these issues, the total number of collected samples is typically lower than the number of participants equipped with gyroscope sensors.

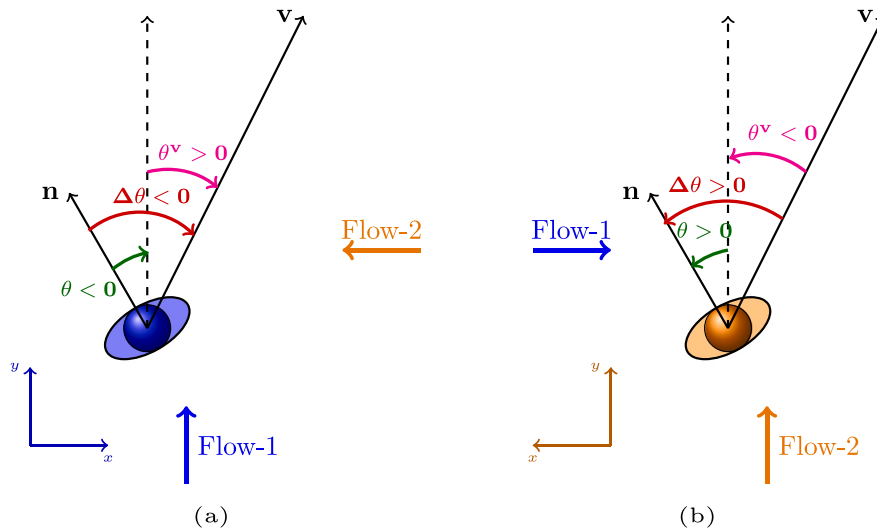The data set is freely available at Feliciani et al. (2022a).

Fig. 2. Graphical definition of observables θ^v, θ and $\Delta\theta$. θ is defined as the angle between the normal to the pedestrian chest **n** and the corridor axis y corresponding to the pedestrian's flow. θ^v is defined as the angle between the velocity **v** and y, while $\Delta\theta$ is defined as the (modulo 2π) difference between θ and $\Delta\theta$. Angles are defined as positive when spanning in the direction of the x axis, the latter showing the direction from which the crossing pedestrians are coming. To better clarify the definition, (a) shows the angle definitions for pedestrians that see the crossing flow as in-coming from their right, while (b) shows the angle definitions for pedestrians that see the crossing flow as in-coming from their left. Arrows starting from the y axis represent positive angles, arrows ending on the y axis negative ones.

Participants equipped with a tablet were given a cap with a different colour, allowing the coupling of their trajectory (obtained from the camera) with body orientation (from the gyroscope sensor). For example, it is possible to know that the participant wearing a green cap and a grey T-shirt and coming from the left (as seen in Fig. 1) was using tablet no. 2 and thus it is possible to study its position and body orientation separately.

Finally, synchronisation between tracking data and body orientation obtained from gyroscope sensors was achieved using a common reference time. Tablets continuously streamed local time and angular speed data to a computer connected to a monitor showing time and experiment number (seen in the upper-left corner of Fig. 1). The information stored in the computer connecting all tablets and the time shown in the video allowed to synchronise trajectories and body orientation with an error of a single video frame, i.e. around 0.03 s. For details on this synchronisation method readers are referred to Feliciani and Nishinari (2022).

3. Observables

In our work we use 9 observables to quantify cross-flow dynamics. In this section, we introduce them providing a qualitative description of their definition and meaning, while a detailed, operative and quantitative definition is provided in Appendix A.

1. The *density in the crossing area* $\rho(t)$ is the time dependence of the number of pedestrians tracked at each time in the crossing region divided by the area of such region, and it is measured in ped/m^2. This is the only *macroscopic* (i.e., defined at the crowd-level, and not at the individual pedestrian-level) observable that we use. Nevertheless, it is strongly related to a microscopic observable, the *exit time* (from the tracking area) E_t, and we will sometimes refer also to the latter observable because it allows for a more straightforward definition of a probability distribution.
2. By v we denote the *pedestrian speed*, whose probability distribution is denoted with $P(v)$, a notation used also for all other pedestrian-level (microscopic) observables defined below.
3. To investigate also the direction of the pedestrian velocity, we study the *velocity direction angle* θ^v. This angle, defined in detail in Appendix A, assumes values in $[-\pi, \pi)$, $\theta^v = 0$ denoting movement along the corridor axis. The angle is defined in such

a way that $\theta^v > 0$ denotes angles in the direction the other flow is coming from. Fig. 2 explains in a graphical way the definition of θ^v and its relation to other observables.

4. A subset of ten subjects was carrying a sensor that allowed us to know their *body orientation*. This is denoted with θ, assuming values in $[-\pi, \pi)$. Here $\theta = 0$ corresponds to the state in which the normal to the pedestrian chest is aligned with the corridor's axis. Again, $\theta > 0$ denotes angles in the direction the other flow is coming from. Refer again to Fig. 2 for a graphical explanation of the definition of θ and its relation to other observables.
5. The *difference between θ and θ^v* is defined as $\Delta\theta$ in such a way that, again, $-\pi \leq \Delta\theta < \pi$. Refer again to Fig. 2.
6. For all pedestrians we also measure, as a vector, the distance to their first neighbours, distinguishing between neighbours in the same flow and in the crossing flow (see Eq. (A.22), (A.24) and Fig. 3). In order to identify the presence of a self-organising pattern, neighbours are defined to be other pedestrians *on the front* of the pedestrian under consideration, i.e., located in the direction of motion, as identified by the corridor's axis. In such a way, if a stripe pattern emerges, there will be a peak in the relative angle distribution corresponding to the stripe axis (if also neighbours on the back were present such peak would be duplicated by symmetry).
   The *magnitude of the relative distance to the first neighbour in the same flow* is denoted as δ^s,
7. while the *magnitude of the relative distance to the first neighbour in the crossing flow* is denoted as δ^o.
8. The angles that these distance vectors form with the corridor axis are, respectively, the *same flow first neighbour relative angle* ϕ^s
9. and *crossing flow first neighbour relative angle* ϕ^o. These angles are defined to assume values in $[-\pi/2, \pi/2]$, $\phi = 0$ identifying the corridor axis and $\phi > 0$ the direction the other flow is coming from (refer again to Fig. 3 for a graphical explanation).

The names, symbols and references to the mathematical definitions of all observables are summarised in Table 2.
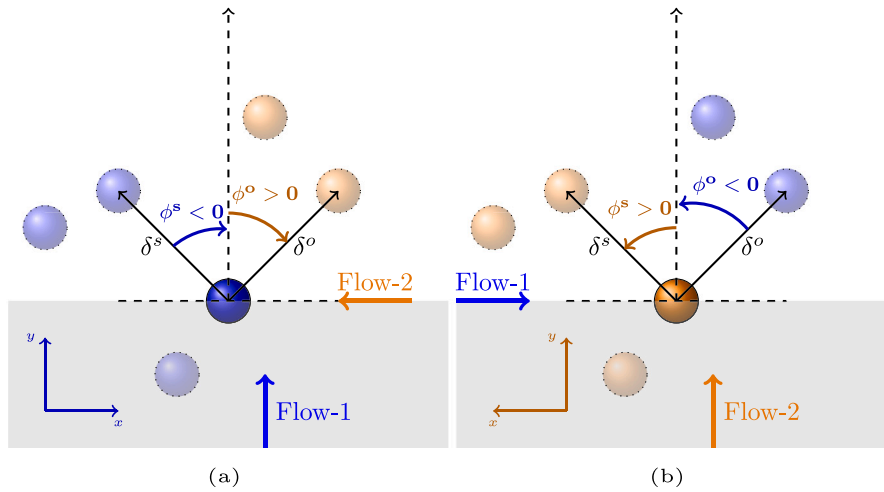
Fig. 3. Graphical definition of observables δ^s, δ^o and ϕ^s and ϕ^o. First neighbours are defined as "the closest pedestrian in the direction of motion", i.e. in the growing y directions (thus the dashed grey area is ignored), and differentiated as belonging to the same or opposite flows. Angle signs are defined as in Fig. 2.
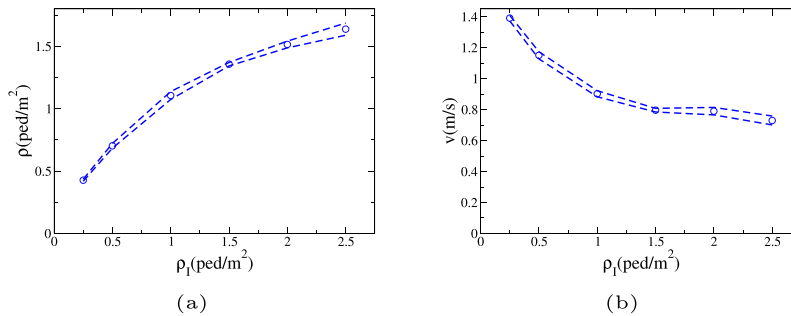

Fig. 4. (a): $\langle \rho \rangle^{\rho_I}$. (b): $\langle v \rangle^{\rho_I}$. Dashed lines provide standard error intervals.

Table 2
Summary of observables.

Name	Symbol	Definition
Density in the crossing area	ρ	Eq. (A.15)
Exit time	E_t	Eq. (A.18)
Pedestrian speed	v	Appendix A.2
Velocity direction angle	θ^v	Eq. (A.19)
Body orientation	θ	Eq. (A.20)
Difference between θ and θ^v	$\Delta\theta$	Eq. (A.21)
Distance to the first neighbour in the same flow	δ^s	Eq. (A.23)
Distance to the first neighbour in the crossing flow	δ^o	Eq. (A.25)
Same flow first neighbour relative angle	ϕ^s	Eq. (A.26)
Crossing flow first neighbour relative angle	ϕ^o	Eq. (A.27)

4. Dependence of observables on density

4.1. Dependence of observables on the initial density ρ_I

For each observable O, we compute its dependence on the initial condition density ρ_I, denoted as $\langle O \rangle^{\rho_I}$ (for a detailed operational definition of these average values and their standard errors and deviations, refer to Appendix B.1).

$\langle \rho \rangle^{\rho_I}$ is reported in Fig. 4(a). Furthermore, the dependence on ρ_I of v is shown in Fig. 4(b), that of the δ observables in Fig. 5(a), that of the ϕ observables in Fig. 5(b), and finally the one of θ observables in Fig. 6(a). We also report in Fig. 6(b) the absolute value of the θ observables (as θ observables are expected to be almost symmetric, their average provides information on their asymmetry, while the average of the absolute value provides information on their spread around 0).

We may observe from Fig. 4(a) that, as expected, ρ is an increasing function of ρ_I. Nevertheless, while at $\rho_I = 0.25$ ped/m^2 we have $\rho \approx 2\rho_I$, at $\rho_I = 2.5$ ped/m^2 we have $\rho \approx 3/5\rho_I$ (this is the average value over the experiment; maxima, as shown in Section 5, in which we report pdfs, are considerably higher, in particular for high ρ_I, although the growth is still sub-linear). We observe (from Figs. 4(b) and 5(a)) that v, δ^o and δ^s are decreasing functions of ρ_I, although they reach a plateau around $\rho_I \approx 1.5$ ped/m^2. We also observe (Fig. 5(b)) that ϕ^s is clearly biased towards positive values. This result, which is related to the "diagonal stripe formation" and it is better discussed studying full pdfs (see again Section 5), is particularly strong in the 1–2 ped/m^2 range. A weaker bias towards positive values is shown also by ϕ^o (Fig. 5(b)).

As seen in Fig. 6(a), the observable $\Delta\theta$ appears to be weakly biased towards negative values, while θ and in particular θ^v are more symmetric. As the signs of the θ observables are defined with respect to the direction the other flow is coming from (as explained in Fig. 2), we expect this result to be related to the experimental setting more than to an actual bias in the left/right symmetry of pedestrian behaviour.

Finally, $|\theta|$ has no clear dependence on ρ_I, while $|\theta^v|$ and $|\Delta\theta|$ are clearly increasing with ρ_I (Fig. 6(b)).

4.2. Dependence of other observables on ρ

The most straightforward way to analyse the results of our experiments is to study the dependence of all observables on the initial density condition ρ_I, as reported in 4.1. We nevertheless noticed that results are more clearly interpreted if the remaining observables are studied as a function of the crossing area density ρ (denoted for each observable O as $\langle O \rangle^\rho$, refer to Appendix B.2 for the detailed operative
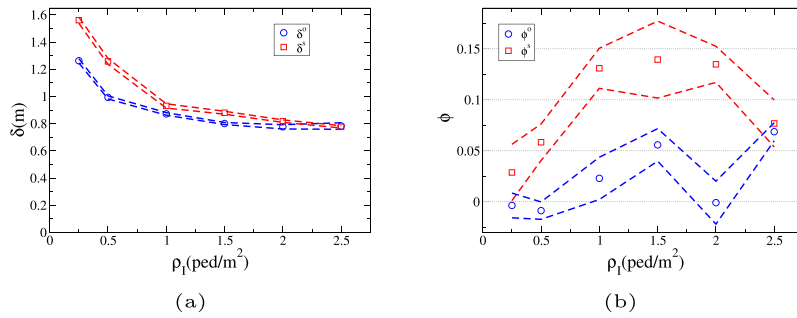
Fig. 5. (a): $\langle\delta^o\rangle^{\rho_I}$ (blue circles) and $\langle\delta^s\rangle^{\rho_I}$ (red squares). (b): $\langle\phi^o\rangle^{\rho_I}$ (blue circles) and $\langle\phi^s\rangle^{\rho_I}$ (red squares). Dashed lines provide standard error intervals.
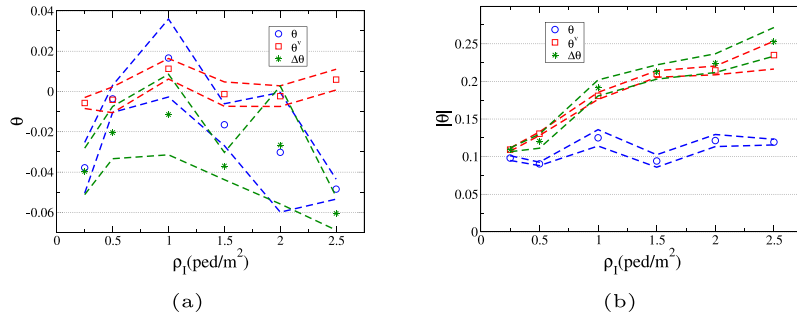

Fig. 6. (a): $\langle\theta\rangle^{\rho_I}$ (blue circles) and $\langle\theta^v\rangle^{\rho_I}$ (red squares) and $\langle\Delta\theta\rangle^{\rho_I}$ (green stars). (b): $\langle|\theta|\rangle^{\rho_I}$ (blue circles) and $\langle|\theta^v|\rangle^{\rho_I}$ (red squares) and $\langle|\Delta\theta|\rangle^{\rho_I}$ (green stars). Dashed lines provide standard error intervals.
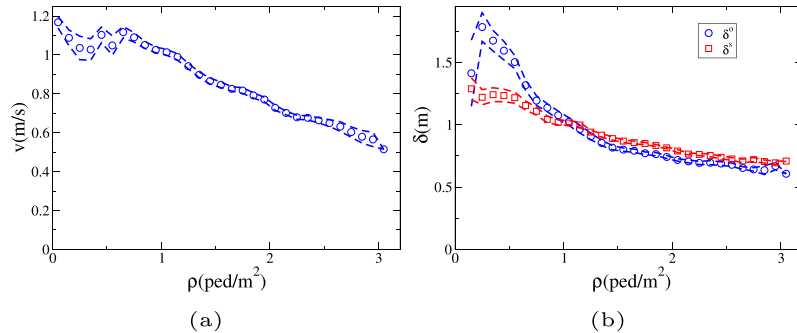

Fig. 7. (a): $\langle v\rangle^{\rho}$. (b): $\langle\delta^o\rangle^{\rho}$ (blue circles) and $\langle\delta^s\rangle^{\rho}$ (red squares). Dashed lines provide standard error intervals.

definition). Indeed, it is not surprising that the dynamics of the crowd is more directly determined by the actual density than by the initial density conditions, and thus we perform such analysis in this section.

The dependence on ρ of v is shown in Fig. 7(a), that of the δ observables in Fig. 7(b), that of the ϕ observables in Fig. 8(a), and that of θ observables in Fig. 8(b). We also report in Fig. 8(c) the absolute value of the θ observables.

In Fig. 7(a) observable v presents an initial plateau for low density, but from $\rho \approx 0.7$ it turns into a decreasing function of ρ, a trend that does not change up to 3 ped/m². Such results are in line with the usual "fundamental diagram" behaviours (compare to the less clear behaviour when v is studied as a function of ρ_I in Fig. 4(b)). Also δ^o and δ^s are decreasing functions of ρ up to 3 ped/m², although they seem to be converging to a stable value (compare again to Fig. 5(a), in which a plateau is reached at $\rho_I \approx 1.5$ ped/m²).

In Fig. 8(a) a bias towards positive values of ϕ^s emerges in a stable way for $\rho > 1.2$ ped/m². As stated above, this result is related to the "diagonal stripe formation" and it is better discussed studying overall pdfs (see Section 5). A weaker bias towards positive values is shown also by ϕ^o for high ρ values (and more strongly but also less regularly for low ρ values).

In Fig. 8(b) observables θ and $\Delta\theta$ are weakly biased towards negative values, while θ^v is weakly biased towards positive ones, although such biases emerge mostly only at high densities (i.e., high values of ρ).

In Fig. 8(c) observables $|\theta^v|$ and $|\Delta\theta|$ are clearly increasing functions of ρ. Also $|\theta|$ appears to grow with ρ, although not as strongly as $|\theta^v|$ and $|\Delta\theta|$. Interestingly, such a pattern for $|\theta|$ does not clearly emerge when this observable is studied as a function of ρ_I in Section 4.1 (see Fig. 6(b)).

5. Overall pdfs

In Figs. 9∼14 we show the results concerning all observables for the $\rho_I = 0.25, 0.5, 1$ and 2 ped/m² initial conditions.

We may see in Fig. 9(a) that the maximum density in the crossing area grows with the initial density. Nevertheless, while it attains a value doubling the initial condition for $\rho_I = 0.25$ ped/m², it is just ≈ 1.25 fold the initial condition at $\rho_I = 2$ ped/m².

Fig. 9(b) shows that the total time for the crowd to pass the crossing area decreases with time, i.e., the flow is increased. Nevertheless, an 8 fold increase in the initial condition density (corresponding to a 5 fold increase in peak density) results in half "passing time".
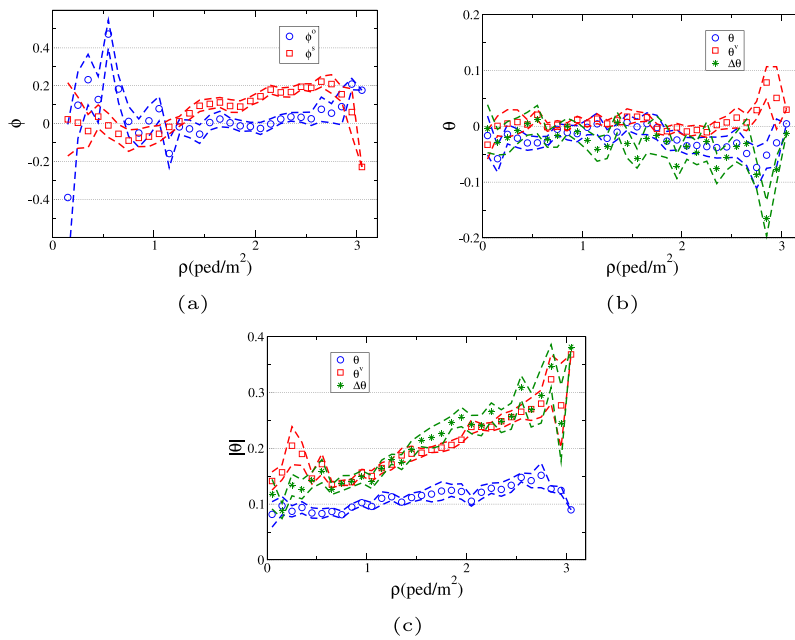
Fig. 8. (a): $\langle\phi^o\rangle^\rho$ (blue circles) and $\langle\phi^s\rangle^\rho$ (red squares). (b): $\langle\theta\rangle^\rho$ (blue circles) and $\langle\theta^v\rangle^\rho$ (red squares) and $\langle\Delta\theta\rangle^\rho$ (green stars). (c): $\langle|\theta|\rangle^\rho$ (blue circles) and $\langle|\theta^v|\rangle^\rho$ (red squares) and $\langle|\Delta\theta|\rangle^\rho$ (green stars). Dashed lines provide standard error intervals.
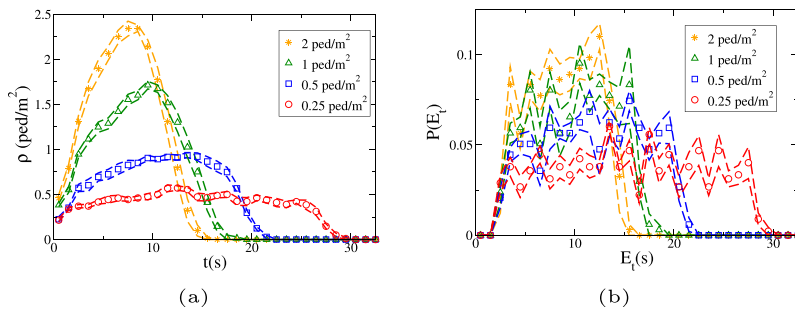

Fig. 9. (a): $\rho(t)$ for different initial conditions. (b): $P(E_t)$ for different initial conditions. Dashed lines provide standard error intervals (computed over independent repetitions).

This finding is obviously related to the decrease in velocity with increasing density, shown in Fig. 10(a), as the velocity peak decreases from ≈ 1.4 m/s for the $\rho_I = 0.25$ ped/m^2 initial condition to ≈ 0.6 m/s for $\rho_I = 2$ ped/m^2.

As shown in Fig. 10(b), motion becomes less ordered as density increases (i.e., the spread of θ^v increases).

In an equivalent way, at high density, it is more probable to have large deviations between the body orientation and the corridor axis (Fig. 11(a)), as well as between the body orientation and the velocity one (Fig. 11(b)). It is nevertheless to be noticed that $|\theta|$ seems to be strongly limited[5] by $\pi/4$, and $|\Delta\theta|$ by $\pi/2$.

The distance between pedestrians in the same flow (Fig. 12(a)) decreases with density, having a peak at ≈ 1.5 m for the $\rho_I = 0.25$ ped/m^2 initial condition, and at ≈ 0.5 m for $\rho_I = 2$ ped/m^2. At the highest initial density condition, the peak attains a similar value also

for the distance to pedestrians in the other flow, while at low density pedestrians get closer to people in the other flow than they do to people in their own flow (peak at ≈ 1 m, Fig. 12(b)).

Finally, we may see (Fig. 13) that, although the angle to the first neighbour in the same flow is skewed to $\phi^s > 0$ for all initial conditions, assuming a maximum at $\approx \pi/4$, in the transition from low to high densities there is a strong decrease in the probability of pedestrians following each other (i.e., having $\phi^s \approx 0$). As the ϕ^s probability distribution presents a peak at an angle $\approx \pi/4$ for all values of ρ_I, we may say that diagonal stripes seem to emerge even at low density, although the phenomenon is stronger at higher densities.

The ϕ^o distribution, shown in Fig. 14, is, compared to the ϕ^s one, less dependent on ρ_I and less noisy. Also the distribution of this variable suggests the presence of a geometrical structure (stripes), with minima at $\approx \pi/4$ (corresponding to the position of a pedestrian from the same flow in case of a diagonal lane Naka, 1977; Mullick et al., 2022).

6. Comments and conclusions

Most of these results are qualitatively intuitive, although they had not, to the limits of our knowledge, been investigated before in a quantitative way. It was expected that the two flows would exhibit some kind of organisation that would regulate the density in the crossing area (Figs. 4(a) and 9), although the quantitative behaviour was not known
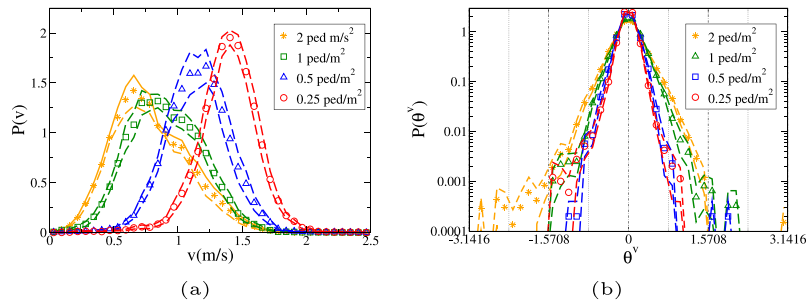
---

[5] When comparing the θ^v distributions of Fig. 10(b) to the θ distributions of Fig. 11(a), two considerations concerning the nature of these observables have to be taken in account. First of all, θ^v may be computed for all subjects, while θ (and thus $\Delta\theta$) only for those provided with a tablet. As a result, the θ^v data set is roughly 6 times larger. It is clear that observations with $|\theta^v| \approx \pi$ refer to subjects without tablet, otherwise larger deviations in the θ and/or $\Delta\theta$ distributions would be observed. Second, as θ^v is computed by differentiating trajectory data, while θ is computed by integrating angular velocity ones, the former is necessarily more noisy than the latter.

Fig. 10. (a): $P(v)$ for different initial conditions. (b): $P(\theta^v)$ for different initial conditions. Dashed lines provide standard error intervals (computed over independent repetitions).
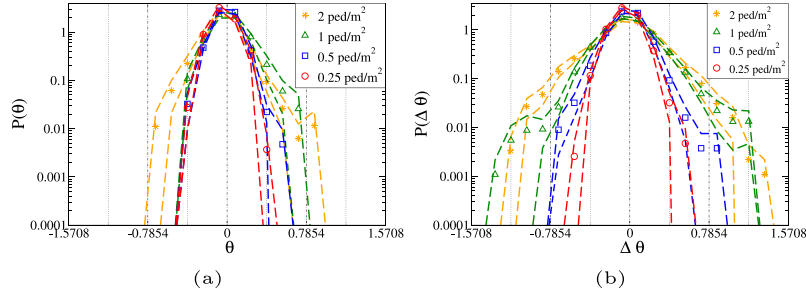

Fig. 11. (a): $P(\theta)$ for different initial conditions. (b): $P(\Delta\theta)$ for different initial conditions. Dashed lines provide standard error intervals (computed over independent repetitions).
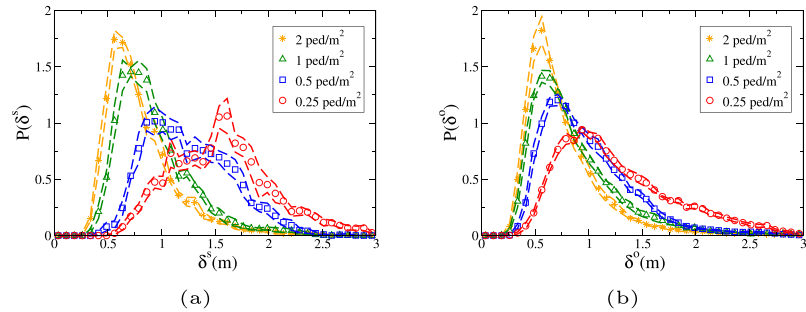

Fig. 12. (a): $P(\delta^s)$ for different initial conditions. (b): $P(\delta^o)$ for different initial conditions. Dashed lines provide standard error intervals (computed over independent repetitions).
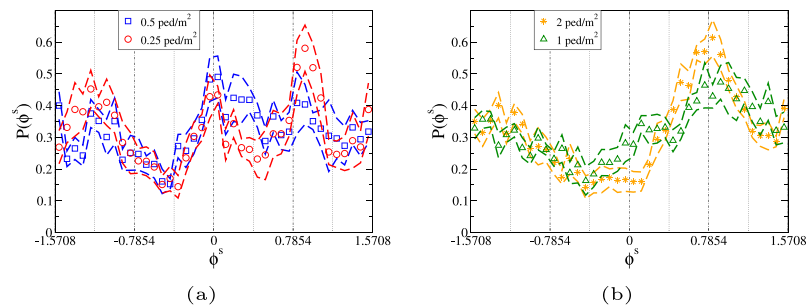

Fig. 13. (a), (b): $P(\phi^s)$ for different initial conditions. Dashed lines provide standard error intervals (computed over independent repetitions).

in advance. Similarly, the velocity/density relation (see in particular Fig. 7(a)) is qualitatively similar to those observed in uni-directional flows. At higher densities, due to an increase in collision avoidance behaviours, we naturally expect more variation in the velocity direction $|\theta^v|$, and this is confirmed by the findings reported in Figs. 6(b), 8(c) and 10(b). Also, the dependence on density (either in the crossing area or as initial conditions) of the distance between pedestrians, follows the expected qualitative behaviour (Figs. 5(a), 7(b) and 12).

The other observables deserve more attention. The ϕ observables are related to the formation of "stripes" in the crossing area. The most intuitive and geometrically straightforward way to identify the stripes

is to notice the $\approx \pi/4$ peak in ϕ^s (Fig. 13), which shows that there is a tendency to have the forward first neighbour in the same flow walking at such an angle in the direction from which the crossing flow is coming (see also the bias towards positive values in Figs. 5(b) and 8(a)). This phenomenon has been shown to happen in many models, and had been reported in the literature (Naka, 1977; Ando et al., 1988; Helbing et al., 2005), but without quantitative data support (although a very recent result has investigated the relation between stripe orientation and crossing angle Mullick et al., 2022). We believe that this aspect of the dynamics deserves to be studied more in detail using clustering algorithms and the like, but since that approach is quite different
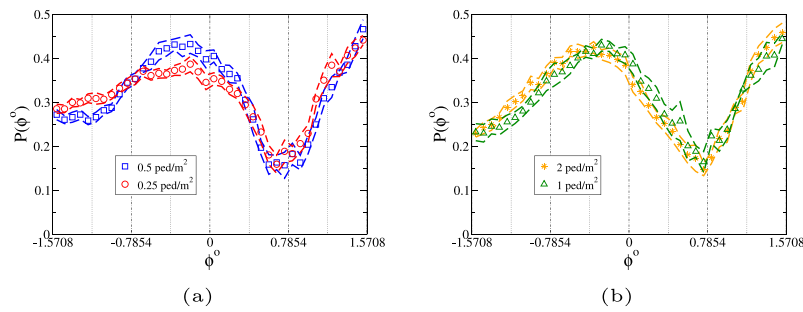
Fig. 14. (a), (b): $P(\phi^o)$ for different initial conditions. Dashed lines provide standard error intervals (computed over independent repetitions).

from the one of this work (relying on straightforward geometrical observables) we leave it for a future work. Nevertheless, since we are not aware of previous experimental results on the dependence of stripe formation on density, we may further comment on this point. From Figs. 5(b), 8(a) and 13 it appears that while the phenomenon is present at any (studied) density, it is definitely stronger at densities (initial or in the crossing area) higher than 1 ped/m^2. It also appears that the stripe formation gets weaker at higher densities, namely at values $\approx 2.5 \sim 3$ ped/m^2, although this effect deserves further study since we obtained few data points at those densities.

It was also expected that, as density grows, $\Delta\theta$ would increase. Nevertheless, as many models do not include the possibility of a discrepancy between velocity and body orientation (if they include body orientation at all), it is very important to quantify this behaviour. We may see that at most densities, $|\theta^v| \approx |\Delta\theta|$ (Figs. 6(b) and 8(c)). Obviously, this does not imply that $|\theta| \approx 0$, but we have indeed verified that $|\theta|$ depends very weakly on initial density conditions (Fig. 6(b)). The situation is more subtle when the relation between $|\theta|$ and ρ is analysed, as we may see that $|\theta|$ increases at high densities (Fig. 8(c)). Similarly, when pdfs are investigated (Fig. 11), we see that at high (initial condition) densities, rare events with large $|\theta|$ are more probable. In a following work (Zanlungo et al., 2022), we will try to understand how important θ is in reproducing the cross-flow dynamics.

Finally, the asymmetry in the θ observable (Figs. 6(a) and 8(b)) is definitely an interesting, although weak, phenomenon. The cross-flow setting is obviously asymmetrical, although to understand whether this is enough to cause the asymmetry in the θ observables, or whether this is due to other aspects of the experimental setting (or to a left/right asymmetry in human behaviour), a comparison with (future) other similar experiments may be necessary.

CRediT authorship contribution statement

Francesco Zanlungo: Conceptualization, Formal analysis, Investigation, Methodology, Software, Validation, Visualization, Writing – original draft, Writing – review & editing. **Claudio Feliciani:** Conceptualization, Data curation, Writing – original draft, Writing – review & editing. **Zeynep Yücel:** Visualization, Writing – original draft, Writing – review & editing. **Katsuhiro Nishinari:** Funding acquisition, Writing – original draft, Writing – review & editing. **Takayuki Kanda:** Funding acquisition, Writing – original draft, Writing – review & editing.

Data availability

We made the data available through the Julich Pedestrian Dynamics Data Archive Feliciani et al. (2022a).

Acknowledgements

Appendix A. Definition of observables

We provide a detailed definition of the observables used in this work. We start with some general definitions that will prove to be useful.

The cardinality of a set S is defined as $\#(S)$. Vectors are denoted by boldface, such as $\mathbf{a}$. The standard Euclidean inner (scalar) product between vectors $\mathbf{a}$ and $\mathbf{b}$ is given by

$$(\mathbf{a}, \mathbf{b}), \tag{A.1}$$

and the Euclidean norm by

$$a = (\mathbf{a}, \mathbf{a})^{\frac{1}{2}}. \tag{A.2}$$

As we always deal with 2D vectors, we may consider their vector product as a scalar (given by its projection on the right-handed normal to the plane). Namely, given an arbitrary right handed frame, we define

$$\langle \mathbf{a}, \mathbf{b} \rangle \equiv (\mathbf{a} \times \mathbf{b})_z = a_x b_y - a_y b_x. \tag{A.3}$$

If we are only interested in the absolute value of $\langle \mathbf{a}, \mathbf{b} \rangle$, we need not to worry about the right-handedness of the frame.

We often use the two-value arctan function, defined as

$$\text{atan2}(a, b) = \begin{cases} \arctan\left(\frac{a}{b}\right), & \text{if } b > 0 \\ \arctan\left(\frac{a}{b} + \pi\right), & \text{if } b < 0, a \geq 0 \\ \arctan\left(\frac{a}{b} - \pi\right), & \text{if } b < 0, a < 0 \\ \frac{\pi}{2}, & \text{if } b = 0, a > 0 \\ -\frac{\pi}{2}, & \text{if } b = 0, a < 0 \\ \text{undefined}, & \text{if } b = 0, a = 0. \end{cases} \tag{A.4}$$

In our analysis we will consider only pedestrians that, at a given time t, are located inside a tracking area, which is defined as an L times L square ($L = 3.4$ m), adding a 0.2 m border on the sides of the magenta area in Fig. 1, to take into account the aforementioned absence of hard walls, and as a consequence has an area $A = L^2$. For each pedestrian i located inside the tracking area (at a given tracking time t) we define the position vector $\mathbf{r}_i$ as the vectorial distance from the origin (e.g., located in the centre of the crossing area). The distance between two pedestrians is defined as

$$\mathbf{r}_{i,j} = \mathbf{r}_j - \mathbf{r}_i. \tag{A.5}$$

At each time t, we also define $f^1(t)$ and $f^2(t)$ as the subset of (tracked) pedestrians belonging, respectively, to flow 1 and 2. Since these sets correspond to tracked pedestrians, they formally depend on tracking time t, although such a dependence is shown only when needed. Their union is the set of tracked pedestrians

$$T(t) = f^1(t) \cup f^2(t). \tag{A.6}$$

Each flow belongs to a corridor, whose axis direction (oriented as the marching direction of the pedestrians, i.e., their goal) is defined

through the normalised vector $\mathbf{j}^k$, $k = \{1, 2\}$. We also define the orthogonal normalised vectors as $\mathbf{i}^1 = -\mathbf{j}^2$, $\mathbf{i}^2 = -\mathbf{j}^1$. It should be noted that, through this definition, $\{\mathbf{i}^k, \mathbf{j}^k\}$ are not necessarily right-handed. This decision is made because we want $\mathbf{i}^k$ to identify the direction the other flow is coming from, in order to have, by symmetry, the same expected distributions for the relative angle observables to be defined below (see also Figs. 2, 3).

Furthermore, for each corridor k, we define a reference frame using

$$a_x^k = (\mathbf{a}, \mathbf{i}^k) \quad a_y^k = (\mathbf{a}, \mathbf{j}^k), \tag{A.7}$$

($a_{x,y}^k$ being the components of an arbitrary vector $\mathbf{a}$ in frame k) and for each pedestrian i, we define the function

$$F(i) = \begin{cases} 1, & \text{if } i \in f^1 \\ 2, & \text{if } i \in f^2. \end{cases} \tag{A.8}$$

An *empirical probability distribution*[6] of an observable O is computed by defining a bin size

$$\Delta O = \frac{O_{\max} - O_{\min}}{n_b}, \tag{A.9}$$

where n_b is the number of bins, and $O_{\min}$, $O_{\max}$ define the interval in which we study the observable distribution.

The number of observations belonging to a bin j is then defined as

$$\begin{aligned} n_j^O = \#(\text{ observations } k \text{ with value } O_k \\ \text{such that } j\Delta O + O_{\min} \le O_k < (j+1)\Delta O + O_{\min}) \end{aligned} \tag{A.10}$$

and the empirical probability distribution of O is

$$P(O) = P\left(\left(j + \frac{1}{2}\right)\Delta O + O_{\min}\right) \equiv P_j = \frac{n_j^O}{\sum_l n_l^O}. \tag{A.11}$$

All empirical probability distributions considered in this work are computed by using $n_b = 40$ bins.

For each experimental condition we performed n_e independent repetitions. In graphs, we compare averages and standard errors over all independent repetitions.

Namely, if P_j^k is the value assumed by the jth bin of a given observable with an experimental condition in the kth independent repetition, graphs will show average values and standard errors

$$\langle P_j \rangle \pm \epsilon_j, \tag{A.12}$$

defined according to

$$\langle P_j \rangle = \frac{\sum_{k=1}^{n_e} P_j^k}{n_e}, \tag{A.13}$$

and

$$\langle (P_j)^2 \rangle = \frac{\sum_{k=1}^{n_e} (P_j^k)^2}{n_e},$$
$$\epsilon_j = \sqrt{\frac{\langle (P_j)^2 \rangle - \langle P_j \rangle^2}{n_e - 1}}. \tag{A.14}$$

A.1. Density $\rho(t)$

The density $\rho(t)$ is the density of pedestrians in the crossing area as a function of time, and it is measured in ped/m². The formal and computational definition is the following. A bin size ΔT_ρ is defined (in the following, we use $\Delta T_\rho = 1$ s). For each instant $t_k = k\delta t_{\text{track}}$ at which tracking was performed ($\delta t_{\text{track}} = 1/30$ s being the tracking time interval, and $k \in \mathbb{N}$), the number of pedestrians in the tracking area

is defined as $n_k = \#(T(t))$. We define the set M_j as consisting of all observation times k such that $j\Delta T_\rho \le k(\delta t_{\text{track}}) < (j+1)\Delta T_\rho$. The density in the crossing area is then defined as

$$\rho(t_j) = \rho\left(\left(j + \frac{1}{2}\Delta T_\rho\right)\right) = \frac{\sum_{k \in M_j} n_k}{A \#(M_j)}, \tag{A.15}$$

$A = L^2$ being the size of the crossing area.

A.1.1. Exit time pdf $P(E_t)$

Between all the observables considered in this work, ρ is the only one that is not defined as a probability density function. As in Zanlungo et al. (2022) we intend to calibrate pedestrian models by comparing simulated pdfs to empirically observed ones by using Earth Mover's Distance, we consider also a corresponding observable which may be defined as a pdf (simply normalising the $\rho(t)$ interval is not a feasible solution, since the absolute value of ρ is of capital importance in pedestrian dynamics).

The chosen observable is the *exit time* pdf $P(E_t)$. Computationally, it is obviously defined using discrete bins. For each observation time $t_k = k\delta t_{\text{track}}$, we define e_k as the number of pedestrians exiting the crossing area, i.e.

$$e_k = \left[\cap_{t' > t_k}(i \notin T(t'))\right] \cap (i \in T(t_k)). \tag{A.16}$$

We then define $\bar{e}_j$ for any bin $t_j = j\Delta T_\rho$ as

$$\bar{e}_j = \sum_{k \in M_j} \#(e_k), \tag{A.17}$$

and finally define the empirical probability distribution of E_t as

$$P(E_t) \equiv P\left(\left(j + \frac{1}{2}\Delta T_\rho\right)\right) \equiv \frac{\bar{e}_j}{\sum_l \bar{e}_l}. \tag{A.18}$$

As all experiment repetitions were finished in less than 40 s, we used 40 bins to define the probability distribution. The same number of bins is used for all the observables, to make comparisons straightforward.

A.2. Speed pdf $P(v)$

Given the velocity $\mathbf{v}_i$ of pedestrian i, v_i gives the pedestrian speed. We consider a possible maximum speed of 2.5 m/s, and in order to have 40 bins we define $\Delta v = 0.0625$ m/s.

A.3. Velocity direction pdf $P(\theta^v)$

We define the velocity direction angle as

$$\theta_i^v = \text{atan2}((v_i)_x^{F(i)}, (v_i)_y^{F(i)}). \tag{A.19}$$

We remind that $(v_i)_{\{x,y\}}^{F(i)}$ are the $\{x, y\}$ components of i's velocity vector as measured in the reference frame corresponding to i's corridor. The function $\text{atan2}(v_x, v_y)$ is chosen in such a way to have $-\pi \le \theta^v < \pi$, with $\theta^v = 0$ for velocities aligned with the corridor's axis, and $\theta^v > 0$ for angles in the direction the other flow is coming from (see also Fig. 2).

The pdf $P(\theta^v)$ is empirically defined by taking bins of size $(2\pi)/40$. Since the angle θ^v is defined with respect to a clear and physically meaningful axis (the corridor direction), and since we verified that the empirical probability distribution is clearly centred around zero and is ≈ 0 for $\theta^v \approx \pm\pi$, all the statistical analysis concerning the observable are performed by treating θ^v (and similarly θ and $\Delta\theta$ to be defined below) as linear (i.e., we are not using circular statistics).

---

[6] The term "distribution" is used since observables are theoretically continuous, although from an empirical point of view they are computed over discrete bins. In general, in figures we normalise them in such a way that their integral equals 1.

A.4. Body direction pdf $P(\theta)$

As explained in Section 2, 10 subjects were carrying a tablet, fixed to their chest. Through a gyroscope, we could know the angular velocity of the tablet, from which (by time integration, and assuming the pedestrians as having their chest orthogonal to the corridor direction as an initial condition) we could obtain the normal unit vector to the chest $\mathbf{n}_i$, and define

$$\theta_i = \mathrm{atan2}((n_i)_x^{F(i)}, (n_i)_y^{F(i)}). \tag{A.20}$$

The pdf $P(\theta)$ is empirically defined by taking bins of size $(2\pi)/40$ (see also Fig. 2).

A.5. Body direction deviation pdf $P(\Delta\theta)$

We also measure the deviation between the body and velocity directions as

$$\Delta\theta_i = \mathrm{Mod}_{2\pi}(\theta_i - \theta_i^v + \pi) - \pi, \tag{A.21}$$

and define again its empirical pdf $P(\Delta\theta)$ by taking bins of size $(2\pi)/40$ (see also Fig. 2).

A.6. Same flow first neighbour relative distance pdf $P(\delta^s)$

For each pedestrian i, we define the *first (forward) neighbour in the same flow* as

$$N_i^s = \arg\min_j r_{i,j}, \text{ with } F(i) = F(j), \text{ and } (\mathbf{r}_{i,j}, \mathbf{j}^{F(i)}) \geq 0. \tag{A.22}$$

We then define the distance to the first neighbour in the same flow as

$$\delta_i^s = r_{i,N_i^s}. \tag{A.23}$$

Namely, δ_i^s is the distance to the closest neighbour in the tracking area belonging to the same flow, *and located on the front* of i (see also Fig. 3).

Considering the size of the crossing area, the empirical pdf $P(\delta_s)$ is defined using bins of size $3/40 = 0.075$ m.

A.7. Crossing flow first neighbour relative distance pdf $P(\delta^o)$

For each pedestrian i, we also define the *first (forward) neighbour in the crossing flow* as

$$N_i^o = \arg\min_j r_{i,j}, \text{ with } F(i) \neq F(j), \text{ and } (\mathbf{r}_{i,j}, \mathbf{j}^{F(i)}) \geq 0, \tag{A.24}$$

and the distance to the first neighbour in the crossing flow as

$$\delta_i^o = r_{i,N_i^o}. \tag{A.25}$$

Namely, δ_i^o is the distance to the closest neighbour in the tracking area belonging to the *crossing* flow, *and located on the front* of i (see also Fig. 3). Also $P(\delta^o)$ is defined using bins of size $3/40 = 0.075$ m.

A.8. Same flow first neighbour relative angle pdf $P(\phi^s)$

For each pedestrian i, we then define

$$\phi_i^s = \mathrm{atan2}((r_{i,N_i^s})_x^{F(i)}, (r_{i,N_i^s})_y^{F(i)}), \tag{A.26}$$

as the relative angle (in i's frame) to the first (forward) neighbour in the same flow. As we require the neighbour to be in the forward position, we have $\phi_i^s \in [-\pi/2, \pi/2]$, and we treat again this observable as a linear one in our statistical analysis. $P(\phi^s)$ is defined using bins of size $\pi/40$. The same considerations apply to ϕ^o defined below (see also Fig. 3).

A.9. Crossing flow first neighbour relative angle pdf $P(\phi^o)$

Finally we define

$$\phi_i^o = \mathrm{atan2}((r_{i,N_i^o})_x^{F(i)}, (r_{i,N_i^o})_y^{F(i)}), \tag{A.27}$$

as the relative angle (in i's frame) to the first (forward) neighbour in the crossing flow.

Appendix B. Definition of observable dependence on density

B.1. Dependence on experimental conditions (initial density ρ_I)

For each initial condition ρ_I, repetition j and observable O, we compute the average value

$$\langle O \rangle_j(\rho_I) \equiv O_j^{\rho_I} \equiv \frac{\sum_{k,l} O_{j,k,l}^{\rho_I}}{\#(\{\rho_I, j\})}, \tag{B.1}$$

where $O_{j,k,l}^{\rho_I}$ stands for the observation concerning pedestrian l at time $k(\delta t_{\mathrm{track}})$ during repetition j with initial condition ρ_I, and $\{\rho_I, j\}$ stands for the whole set of observations concerning repetition j with initial condition ρ_I. Furthermore, we compute the average value for the initial condition as

$$\langle O \rangle^{\rho_I} = \frac{\sum_j O_j^{\rho_I}}{\#(\{\rho_I\})}, \tag{B.2}$$

and the corresponding standard error as

$$\varepsilon_{O^{\rho_I}} = \sqrt{\frac{\langle O^2 \rangle^{\rho_I} - \langle O \rangle^{\rho_I 2}}{\#(\{\rho_I\}) - 1}}. \tag{B.3}$$

Here $\#(\{\rho_I\})$ stands for the number of repetitions with initial condition ρ_I.

B.2. Dependence on crossing area density ρ

While the above discussion allows us to see how the observables depend on the initial condition, equally or even more interesting is to study their dependence on the crossing area density ρ. We may define a density interval $\Delta\rho$ (that for practical purposes is fixed to 0.1 ped/m^2), and denote $\{(m + 1/2)\Delta\rho, j\}$ as the set of observations concerning pedestrian l during repetition j *for all times k such that* $m\Delta\rho \leq \rho_k < (m+1)\Delta\rho$. Then we can proceed as above to obtain

$$\langle O \rangle_j^{\rho} \equiv O_j^{\rho} \equiv \frac{\sum_{k,l} O_{j,k,l}^{\rho}}{\#(\{\rho, j\})}, \tag{B.4}$$

$$\langle O \rangle^{\rho} = \frac{\sum_j O_j^{\rho}}{\#(\{\rho\})}, \tag{B.5}$$

$$\varepsilon_{O^{\rho}} = \sqrt{\frac{\langle O^2 \rangle^{\rho} - \langle O \rangle^{\rho_I 2}}{\#(\{\rho\}) - 1}}, \tag{B.6}$$

where, to simplify the notation, the discrete value $(m+1/2)\Delta\rho$ has been replaced by ρ.

References

Adrian, J., Seyfried, A., Sieben, A., 2020. Crowds in front of bottlenecks at entrances from the perspective of physics and social psychology. J. R. Soc. Interface 17 (165), 20190871. http://dx.doi.org/10.1098/rsif.2019.0871.

Ando, K., Ota, H., Oki, T., 1988. Forecasting the flow of people. Railway Res. Rev. 45 (8), 8–14, (in Japanese).

Bode, N.W., Holl, S., Mehner, W., Seyfried, A., 2015. Disentangling the impact of social groups on response times and movement dynamics in evacuations. PLoS One 10 (3), e0121227. http://dx.doi.org/10.1371/journal.pone.0121227.

Boltes, M., Seyfried, A., 2013. Collecting pedestrian trajectories. Neurocomputing 100, 127–133. http://dx.doi.org/10.1016/j.neucom.2012.01.036.

Boltes, M., Seyfried, A., Steffen, B., Schadschneider, A., 2010. Automatic extraction of pedestrian trajectories from video recordings. In: Pedestrian and Evacuation Dynamics 2008. Springer, pp. 43–54. http://dx.doi.org/10.1007/978-3-642-04504-2_3.

Cao, S., Lian, L., Chen, M., Yao, M., Song, W., Fang, Z., 2018. Investigation of difference of fundamental diagrams in pedestrian flow. Physica A 506, 661–670. http://dx.doi.org/10.1016/j.physa.2018.04.084.

Cao, S., Seyfried, A., Zhang, J., Holl, S., Song, W., 2017. Fundamental diagrams for multidirectional pedestrian flows. J. Stat. Mech. Theory Exp. 2017 (3), 033404. http://dx.doi.org/10.1088/1742-5468/aa620d.

Cao, S., Zhang, J., Salden, D., Ma, J., Shi, C., Zhang, R., 2016. Pedestrian dynamics in single-file movement of crowd with different age compositions. Phys. Rev. E 94 (1), 012312. http://dx.doi.org/10.1103/PhysRevE.94.012312.

Chattaraj, U., Seyfried, A., Chakroborty, P., 2009. Comparison of pedestrian fundamental diagram across cultures. Adv. Complex Syst. 12 (03), 393–405. http://dx.doi.org/10.1142/S0219525909002209.

Cividini, J., Appert-Rolland, C., 2013. Wake-mediated interaction between driven particles crossing a perpendicular flow. J. Stat. Mech. Theory Exp. 2013 (07), P07015. http://dx.doi.org/10.1088/1742-5468/2013/07/P07015.

Cividini, J., Appert-Rolland, C., Hilhorst, H.-J., 2013a. Diagonal patterns and chevron effect in intersecting traffic flows. Europhys. Lett. 102 (2), 20002. http://dx.doi.org/10.1209/0295-5075/102/20002.

Cividini, J., Hilhorst, H., Appert-Rolland, C., 2013b. Crossing pedestrian traffic flows, the diagonal stripe pattern, and the chevron effect. J. Phys. A 46 (34), 345002. http://dx.doi.org/10.1088/1751-8113/46/34/345002.

Crociani, L., Vizzari, G., Yanagisawa, D., Nishinari, K., Bandini, S., 2016. Route choice in pedestrian simulation: Design and evaluation of a model based on empirical observations. Intell. Artif. 10 (2), 163–182. http://dx.doi.org/10.3233/IA-160102.

Feliciani, C., Murakami, H., Nishinari, K., 2018. A universal function for capacity of bidirectional pedestrian streams: Filling the gaps in the literature. PLoS One 13 (12), e0208496. http://dx.doi.org/10.1371/journal.pone.0208496.

Feliciani, C., Murakami, H., Nishinari, K., 2022a. Perpendicular crossflow experiment with partial information on body orientation. http://dx.doi.org/10.34735/ped.2019.2.

Feliciani, C., Murakami, H., Shimura, K., Nishinari, K., 2020a. Efficiently informing crowds–experiments and simulations on route choice and decision making in pedestrian crowds with wheelchair users. Transp. Res. C 114, 484–503. http://dx.doi.org/10.1016/j.trc.2020.02.019.

Feliciani, C., Nishinari, K., 2016. Empirical analysis of the lane formation process in bidirectional pedestrian flow. Phys. Rev. E 94 (3), 032304. http://dx.doi.org/10.1103/PhysRevE.94.032304.

Feliciani, C., Nishinari, K., 2022. Estimation of pedestrian crowds' properties using commercial tablets and smartphones. Transp. B: Transp. Dyn. http://dx.doi.org/10.1080/21680566.2018.1517061.

Feliciani, C., Shimura, K., Nishinari, K., 2022b. Introduction to Crowd Management – Managing Crowds in the Digital Era: Theory and Practice. Springer Nature, http://dx.doi.org/10.1007/978-3-030-90012-0.

Feliciani, C., Zuriguel, I., Garcimartín, A., Maza, D., Nishinari, K., 2020b. Systematic experimental investigation of the obstacle effect during non-competitive and extremely competitive evacuations. Sci. Rep. 10 (1), 1–20. http://dx.doi.org/10.1038/s41598-020-72733-w.

Fruin, J.J., 1971. Pedestrian planning and design, vol.206.

Fujita, A., Feliciani, C., Yanagisawa, D., Nishinari, K., 2019. Traffic flow in a crowd of pedestrians walking at different speeds. Phys. Rev. E 99 (6), 062307. http://dx.doi.org/10.1103/PhysRevE.99.062307.

Geoerg, P., Schumann, J., Holl, S., Hofmann, A., 2019. The influence of wheelchair users on movement in a bottleneck and a corridor. J. Adv. Transp. http://dx.doi.org/10.1155/2019/9717208.

Haghani, M., Sarvi, M., 2018. Crowd behaviour and motion: Empirical methods. Transp. Res. B 107, 253–294. http://dx.doi.org/10.1016/j.trb.2017.06.017.

Helbing, D., Buzna, L., Johansson, A., Werner, T., 2005. Self-organized pedestrian crowd dynamics: Experiments, simulations, and design solutions. Transp. Sci. 39 (1), 1–24. http://dx.doi.org/10.1287/trsc.1040.0108.

Hittmeir, S., Ranetbauer, H., Schmeiser, C., Wolfram, M.T., 2016. Derivation and analysis of continuum models for crossing pedestrian traffic. http://dx.doi.org/10.48550/arXiv.1612.07582, arXiv:1612.07582.

International Organization for Standardization, 2020. ISO 20414: Fire safety engineering – verification and validation protocol for building fire evacuation models.

Jelić, A., Appert-Rolland, C., Lemercier, S., Pettré, J., 2012. Properties of pedestrians walking in line: Fundamental diagrams. Phys. Rev. E 85 (3), 036111. http://dx.doi.org/10.1103/PhysRevE.85.036111.

Lee, R.S., Hughes, R.L., 2005. Exploring trampling and crushing in a crowd. J. Transp. Eng. 131 (8), 575–582. http://dx.doi.org/10.1061/(ASCE)0733-947X(2005)131:8(575.

Lovreglio, R., Ronchi, E., Kinsey, M.J., 2020. An online survey of pedestrian evacuation model usage and users. Fire Technol. 56 (3), 1133–1153. http://dx.doi.org/10.1007/s10694-019-00923-8.

Mullick, P., Fontaine, S., Appert-Rolland, C., Olivier, A.-H., Warren, W.H., Pettré, J., 2022. Analysis of emergent patterns in crossing flows of pedestrians reveals an invariant of 'stripe' formation in human data. PLoS Comput. Biol. 18 (6), e1010210. http://dx.doi.org/10.1371/journal.pcbi.1010210.

Murakami, H., Feliciani, C., Nishiyama, Y., Nishinari, K., 2021. Mutual anticipation can contribute to self-organization in human crowds. Sci. Adv. 7 (12), eabe7758. http://dx.doi.org/10.1126/sciadv.abe7758.

Nagao, K., Yanagisawa, D., Nishinari, K., 2018. Estimation of crowd density applying wavelet transform and machine learning. Physica A 510, 145–163. http://dx.doi.org/10.1016/j.physa.2018.06.078.

Naka, Y., 1977. Mechanism of cross passenger flow - study on complicated passenger flow in railway station (Part I). Trans. Arch. Inst. Jpn. 258, 93–102. http://dx.doi.org/10.3130/aijsaxx.258.0_93, (in Japanese).

Rokko High School, 2017. Rokko high school sport festival 2017: Marching parade. https://youtu.be/Sd5xV5RtF1A?t610.

Seyfried, A., Passon, O., Steffen, B., Boltes, M., Rupprecht, T., Klingsch, W., 2009. New insights into pedestrian flow through bottlenecks. Transp. Sci. 43 (3), 395–406. http://dx.doi.org/10.1287/trsc.1090.0263.

Subaih, R., Maree, M., Chraibi, M., Awad, S., Zanoon, T., 2020. Experimental investigation on the alleged gender-differences in pedestrian dynamics: a study reveals no gender differences in pedestrian movement behavior. IEEE Access 8, 33748–33757. http://dx.doi.org/10.1109/ACCESS.2020.2973917.

Totzeck, C., 2019. An anisotropic interaction model with collision avoidance. http://dx.doi.org/10.3934/krm.2020044, arXiv:1912.04234.

Von Krüchten, C., Schadschneider, A., 2017. Empirical study on social groups in pedestrian evacuation dynamics. Physica A 475, 129–141. http://dx.doi.org/10.1016/j.physa.2017.02.004.

Wang, J., Boltes, M., Seyfried, A., Zhang, J., Ziemer, V., Weng, W., 2018. Linking pedestrian flow characteristics with stepping locomotion. Physica A 500, 106–120. http://dx.doi.org/10.1016/j.physa.2018.02.021.

Weidmann, U., 1993. Transporttechnik Der Fussgänger: Transporttechnische Eigenschaften Des Fussgängerverkehrs ; (Literaturauswertung), Vol. 90. IVT Schriftenreihe.

Willems, J., Corbetta, A., Menkovski, V., Toschi, F., 2020. Pedestrian orientation dynamics from high-fidelity measurements. Sci. Rep. 10 (1), 1–10. http://dx.doi.org/10.1038/s41598-020-68287-6.

Wong, S.C., Leung, W.L., Chan, S.H., Lam, W.H.K., Yung, N.H.C., Liu, C.Y., Zhang, P., 2010. Bidirectional pedestrian stream model with oblique intersecting angle. J. Transp. Eng. 136 (3), 234–242. http://dx.doi.org/10.1061/(ASCE)TE.1943-5436.0000086.

Ye, R., Fang, Z., Lian, L., Wang, Q., Zeng, G., Cao, S., Zhang, J., Song, W., 2021. Traffic dynamics of uni-and bidirectional pedestrian flows including dyad social groups in a ring-shaped corridor. J. Stat. Mech. Theory Exp. 2021 (2), 023406. http://dx.doi.org/10.1088/1742-5468/abdc1a.

Zanlungo, F., Brščić, D., Kanda, T., 2015. Spatial-size scaling of pedestrian groups under growing density conditions. Phys. Rev. E 91 (6), 062810. http://dx.doi.org/10.1103/PhysRevE.91.062810.

Zanlungo, F., Crociani, L., Yücel, Z., Kanda, T., 2020. The effect of social groups on the dynamics of bi-directional pedestrian flow: a numerical study. In: Traffic and Granular Flow 2019. Springer, pp. 307–313. http://dx.doi.org/10.1007/978-3-030-55973-1_38.

Zanlungo, F., Feliciani, C., Yücel, Z., Nishinari, K., Kanda, T., 2022. Macroscopic and microscopic dynamics of a pedestrian cross-flow: part ii, modelling. To be published in Safety Science.

Zanlungo, F., Ikeda, T., Kanda, T., 2012. A microscopic social norm model to obtain realistic macroscopic velocity and density pedestrian distributions. PLoS One 7 (12), e50720. http://dx.doi.org/10.1371/journal.pone.0050720.

Zanlungo, F., Ikeda, T., Kanda, T., 2014. Potential for the dynamics of pedestrians in a socially interacting group. Phys. Rev. E 89 (1), 012811. http://dx.doi.org/10.1103/PhysRevE.89.012811.

Zanlungo, F., Kanda, T., 2015. A mesoscopic model for the effect of density on pedestrian group dynamics. Europhys. Lett. 111 (3), 38007. http://dx.doi.org/10.1209/0295-5075/111/38007.

Zanlungo, F., Yücel, Z., Brščić, D., Kanda, T., Hagita, N., 2017. Intrinsic group behaviour: Dependence of pedestrian dyad dynamics on principal social and personal features. PLoS One 12 (11), e0187253. http://dx.doi.org/10.1371/journal.pone.0187253.

Zanlungo, F., Yücel, Z., Kanda, T., 2019. Intrinsic group behaviour II: On the dependence of triad spatial dynamics on social and personal features; and on the effect of social interaction on small group dynamics. PLoS One 14 (12), e0225704. http://dx.doi.org/10.1371/journal.pone.0225704.

Zhang, J., Klingsch, W., Schadschneider, A., Seyfried, A., 2012. Ordering in bidirectional pedestrian flows and its influence on the fundamental diagram. J. Stat. Mech. Theory Exp. 2012 (02), P02002. http://dx.doi.org/10.1088/1742-5468/2012/02/P02002.